Hindawi Publishing Corporation
Journal of Nanomaterials
Volume 2012, Article ID 674168, 9 pages
doi:10.1155/2012/674168

Research Article

Electrochromic Devices Based on Porous Tungsten Oxide Thin Films

Y. Djaoued,[1] S. Balaji,[1] and R. Brüning[2]

[1] *Laboratoire de Recherche en Matériaux et Micro-Spectroscopies Raman et FTIR, Université de Moncton—Campus de Shippagan, 218 Boulevard J.-D. Gauthier, Shippagan, NB, Canada E8S 1P6*
[2] *Physics Department, Mount Allison University, 67 York Street, Sackville, NB, Canada E4L 1E6*

Correspondence should be addressed to Y. Djaoued, yahia.djaoued@umoncton.ca

Received 29 May 2012; Accepted 22 June 2012

Academic Editor: Vo-Van Truong

Recent developments in the synthesis of transition metal oxides in the form of porous thin films have opened up opportunities in the construction of electrochromic devices with enhanced properties. In this paper, synthesis, characterization and electrochromic applications of porous WO_3 thin films with different nanocrystalline phases, such as hexagonal, monoclinic, and orthorhombic, are presented. Asymmetric electrochromic devices have been constructed based on these porous WO_3 thin films. XRD measurements of the intercalation/deintercalation of Li^+ into/from the WO_3 layer of the device as a function of applied coloration/bleaching voltages show systematic changes in the lattice parameters associated with structural phase transitions in Li_xWO_3. Micro-Raman studies show systematic crystalline phase changes in the spectra of WO_3 layers during Li^+ ion intercalation and deintercalation, which agree with the XRD data. These devices exhibit interesting optical modulation (up to ~70%) due to intercalation/deintercalation of Li ions into/from the WO_3 layer of the devices as a function of applied coloration/bleaching voltages. The obtained optical modulation of the electrochromic devices indicates that, they are suitable for applications in electrochromic smart windows.

1. Introduction

Tungsten oxide (WO_3) has been one of the most widely studied materials due to its multifunctional properties that have wide spectrum of applications in electrochromic devices, catalysers, gas sensors, optical switching devices, and so forth [1–3]. Over the past three decades, intensive research has been carried out towards improving WO_3-based electrochromic (EC) devices due to their important energy saving properties [4–7]. A typical asymmetric EC device consists of an ion conducting (IC) layer, which also acts as a counter electrode and a WO_3 electrochromic layer as the working cathode, sandwiched between two transparent conductive electrodes (TEs) [8, 9]. When a low voltage (1–3 V) is applied across the TEs, Li^+ ions from the counter electrode and electrons (e^-) from the TE move to the EC WO_3 layer. This double injection results in the formation of colored Li_xWO_3 bronzes, with a controllable degree of coloration as a function of x (Li ion concentration). When the applied voltages are reversed, the Li^+ ions deintercalate, leading to a bleached state. The EC phenomenon, with xe^- and Li^+ ions inserted into (ejected out of) the system, can be represented as:

$$\underset{\text{clear}}{WO_3} + x\mathrm{Li}^+ + xe^- \longleftrightarrow \underset{\text{dark blue}}{\mathrm{Li}_xWO_3} \quad (1)$$

The performance of an EC device depends on the crystallinity, crystallite size, porosity, and thickness of the electrochromically active layer [10–14]. As far as the preparation of individual layers in an EC device is concerned, PVD techniques (thermal evaporation, sputtering, pulsed laser deposition) and mild chemical approaches such as sol-gel processes have been used [10–15]. Among these, the sol-gel technique is attractive. The sol-gel process allows a detailed control of the film texture and structure, leading to tailored electrochromic properties. Mesoporous WO_3 films prepared by a sol-gel method with block copolymer templates have been investigated by Cheng et al. and by Djaoued et al. [11, 14]. Macroporous WO_3 films were also synthesized via

sol-gel processing using polyethylene-glycol as a templating agent [12]. Mesoporous materials, due to their higher surface area, exhibit better kinetics for coloration and bleaching in comparison with standard sol-gel-derived WO_3 thin films. On the other hand, macroporous WO_3, which may have a wider range of applications as an ion hosting material, has displayed coloration efficiency values higher than those previously reported in the literature [12]. The motivation for synthesizing such porous materials emerges from the increased diffusion constant of intercalating ions by two orders of magnitude in porous EC-layer-based devices. Templating agents such as polyethyleneglycol (PEG), pluronic (P123), or organically modified silane (ORMOSIL) increase the porosity of the electrochromic layer [8, 9]. In addition to that ORMOSIL has certain other advantages upon annealing, as the silane in the ORMOSIL provides a silica network which helps to prepare crack-free WO_3 films. Crystalline phases of WO_3 occur primarily in three forms: distorted cubic ReO_3 structures, hexagonal, and pyrochlore. The distorted cubic ReO_3 structure manifests itself, in monoclinic (Pc), triclinic (P1), monoclinic (P21/n), orthorhombic (Pmnb), and tetragonal (P4/nmm) phases at various temperatures ranging from -263 to 900°C, in increasing order of symmetry. Usually electrochromic studies have been performed on hexagonal (h), pyrochlore, and monoclinic (m) phases as they are naturally stable or metastable at room temperature [4, 8, 9, 16, 17]. Another factor that influences the performance of the electrochromic devices is the nanostructures of WO_3. A detailed study of electrochromic properties of nanostructured tungsten oxide with room temperature stable structure of m-WO_3, metastable structure of h-WO_3, and titania-stabilized o-WO_3 (higher temperature phase) has not been published until recently. Another interesting aspect is the phase changes that are associated with the electrochromic effect in crystalline WO_3. Intercalation of Li into ReO_3 type tungsten oxides transforms lower symmetry phases to the higher symmetry phases. This phase change has been studied by Raman spectroscopy or by XRD by many researchers [16–19].

When both Raman spectroscopy and XRD techniques are employed simultaneously, a detailed study of the intermediate structural changes in the Li_xWO_3 can be performed. These methods are practical for the device characterization as they can be performed nondestructively, they can probe the structural changes occurring in the EC layer and provide an estimate of the quantity of intercalated ions.

In this paper, we present a sol-gel methodology based on tungstic acid in the presence of ORMOSIL as a templating agent to prepare films of nanostructured hexagonal-WO_3, nanostructured monoclinic-WO_3, and titania-stabilized orthorhombic WO_3 with mesomacroporous features. These phases have been stabilized as thin films and used as an active electrochromic layers for the construction of asymmetric electrochromic devices. A detailed micro-Raman spectroscopic structural characterization of Li ions intercalation/deintercalation into the WO_3 layer of the operating EC devices as a function of applied coloration/bleaching voltages has been performed. Results of the XRD characterization of the structural changes occurring during the intercalation/deintercalation of Li ions into the WO_3 layers of the operating EC device as a function of applied voltages are described. The optical transmittance data obtained in conjunction with the Raman and the XRD studies are presented to demonstrate the applicability of these materials for energy saving electrochromic smart windows.

2. Experimental Details

In order to obtain porous WO_3 films with sufficient thickness, hybrid organically modified silicates (ORMOSIL) was used as a template precursor. It was prepared by an acylation reaction between poly(propylene glycol) bis(2-aminopropyl ether) (2-APPG) with isocyanatopropyltriethoxysilane (ICS) in tetrahydrofuran (THF) in the volume ratio 1 : 0.1 : 1 [6, 8, 20].

2.1. Synthesis of h-WO_3 and m-WO_3. The sol-gel coating solutions used for the preparation of h-WO_3 and m-WO_3 films were synthesized according to the following procedures. WO_3 sols were prepared by dissolving tungsten powder (99.9%) in 35% hydrogen peroxide. The mixture was left to stir at room temperature for 8 hours. After the addition of a small amount of ethanol (EtOH), the sol was refluxed for 4 hours at a temperature of 80°C. Finally, 1.5 g of the hybrid ORMOSIL dissolved in EtOH was added dropwise into the WO_3 sol and stirred for one hour. The final sol was used for the WO_3 film coating. The WO_3 films were deposited by dip coating onto SiO_2-coated glass or indium tin oxide (ITO) coated-glass substrates with a surface resistivity of 5–15 Ω/sq, at a controlled speed of 4 mm/s. After drying at 60°C, the films were annealed at 400 and 500°C and were held at the peak temperature for one hour and then cooled to room temperature which resulted in h-WO_3 and m-WO_3, respectively.

2.2. Synthesis of o-WO_3. It has been a challenge to stabilize the higher symmetric phases of WO_3 such as orthorhombic (o), tetragonal (t), and cubic (c) at room temperature, since ReO_3-type WO_3 reverts to m-WO_3, due to a second-order Jahn-teller distortion, irrespective of thermal treatment [21]. A two-stage process was adopted to prepare o-WO_3 thin films on ITO-coated glass substrates. The first stage involves the dip coating of a tungsten oxide film using the above described tungstic acid sol in the presence of ORMOSIL as a templating agent, followed by an annealing at 600°C for one hour, resulting in the formation of a porous WO_3 thin film. In the second stage, the porous WO_3 film was dip coated with a titanium-alkoxide-based ethanol solution containing ORMOSIL, followed by another annealing at 600°C to prepare TiO_2-stabilized o-WO_3 film.

2.3. Fabrication of EC Devices. We prepared several electrochromic devices with the configuration:

$$\text{ITO-coated-glass-1/}WO_3\text{/ICL/ITO-coated-glass-2}, \quad (2)$$

where ITO-coated-glass-1 and ITO-coated-glass-2 are the two transparent electrodes (TEs) used to apply the electric

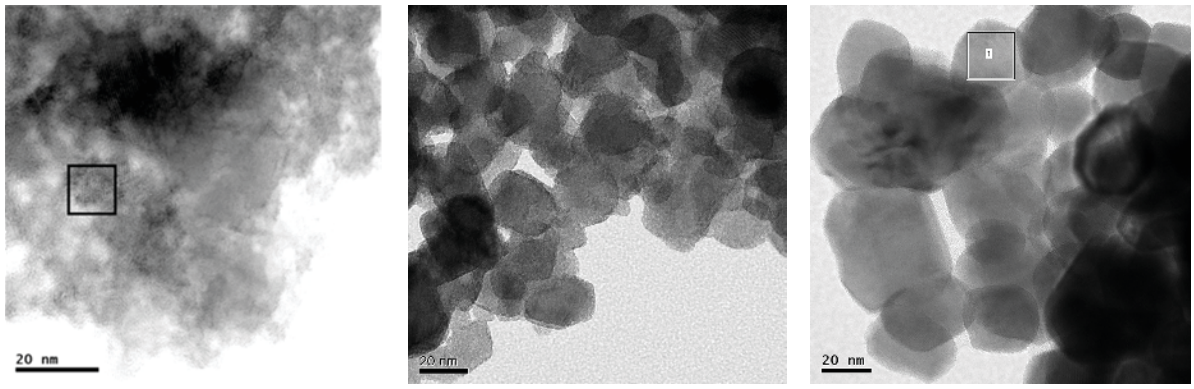

(a) 400°C (b) 500°C (c) 600°C

Figure 1: Transmission electron micrographs of tungsten oxide films prepared at 400 (grain size ~10 nm), 500 (grain size ~19 nm), and 600°C (grain size ~25 nm).

field, WO_3 is the electrochromic layer and ICL is the ion conducting and electronically insulating layer. The ICL is applied on top of the WO_3 layer and the ITO-coated-glass-2 is gently pressed against this coating to ensure a uniform distribution of the ICL. After making the electrical connections, the EC device is ready for testing. The area of the EC devices was $5 \times 2.5\,cm^2$.

2.4. Structural and Optical Characterization

2.4.1. Transmission Electron Microscopy. A WO_3 layer was deposited onto a SiO_2-coated glass substrate and annealed in air at 400, 500, or 600°C for one hour. TEM of the WO_3 layers was performed on a small amount of film scrapped off the SiO_2-coated glass substrate and placed into a glass vial. The sample was imaged using a 2011 JEOL STEM at 200 keV. Images were captured on a 4 k × 4 k multiscan CCD camera using Digital Micrograph from Gatan.

2.4.2. Raman Spectroscopy. Raman spectra were recorded at room temperature with a Jobin-Yvon Labram HR micro-analytical spectrometer equipped with a motorized xy stage and autofocus. The spectra were generated with 17 mW, 632.8 nm He-Ne laser excitation and dispersed with the 1800 grooves/mm grating across the 0.8 m length of the spectrograph. The laser power was 4 mW at the sample surface. The spectral resolution is estimated to be less than $0.5\,cm^{-1}$ for a slit width of 150 μm and a confocal hole of 300 μm.

2.4.3. X-Ray Diffraction (XRD). XRD measurements were carried out in reflection with a custom built theta-theta diffractometer equipped with pyrolytic graphite monochromator and analyzer crystals. Cu K-α radiation (λ = 0.154178 nm) was used for the measurements, and the data are shown as a function of the modulus of the scattering vector $q = 4\pi\lambda^{-1}\sin\theta$, where 2θ is the scattering angle. Air scattering was avoided by evacuating the sample space. We determine the lattice constants for different sample states by fitting the diffraction patterns. Each spectrum is fitted to a series of Gaussian peaks superimposed on an overall quadratic background. These fits, shown as lines in the figure, match the data points closely. The peak width, assumed to be the same for all reflections, and the intensities of the individual peaks are treated as fitting parameters. We correct the peak width for the instrument resolution and use it to estimate the crystallite size using the Scherrer method, assuming that for example, crystallite-to-crystallite variations of the lattice parameter do not contribute to the peak widths.

2.4.4. UV-VIS Spectrophotometery. The optical transmittance spectra of the EC devices in their colored/bleached states were recorded at normal incidence with a Biochrom Ultrospec 2000 UV-visible spectrophotometer.

3. Results and Discussion

3.1. Microstructure of the EC Layer Prepared at Different Temperatures. TEM of the WO_3 layers was performed on a small amount of film scraped off the SiO_2-coated glass substrate. Figure 1(a) shows the TEM image of the nanocrystalline WO_3 annealed at 400°C. The nanocrystalline nature is evident from the dimension of domain which is showing crystalline lattice. The interplanar distances obtained by inverse Fast Fourier transforms (FFTs) of lattice spacing shown in the region indicated by the box were found to be 0.72 and 0.79 nm, respectively. These lattice spacings correspond to those of hexagonal WO_3 (h-WO_3) which are a = 0.7298(2) nm, c = 0.7798(3) nm. Figure 1(b) shows the TEM image for the film annealed at 500°C. The average crystallite size was found to be 19.3 nm. The lattice spacings were determined by the FFT of the lattice fringes at two different points on the WO_3 crystallites (not shown here) and are found to be 0.3658 and 0.3625 nm, again matching m-WO_3. Figure 1(b) also shows the mesoporous structure of the walls separating the macropores in the WO_3 films. Figure 1(c) shows the TEM image of the similarly prepared

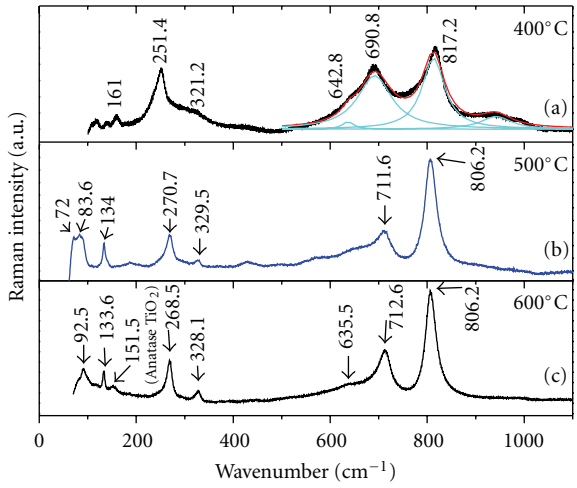

Figure 2: Micro-Raman spectra of tungsten oxide thin films prepared at 400, 500, 600°C indicating the formation of h-WO_3, m-WO_3, and o-WO_3.

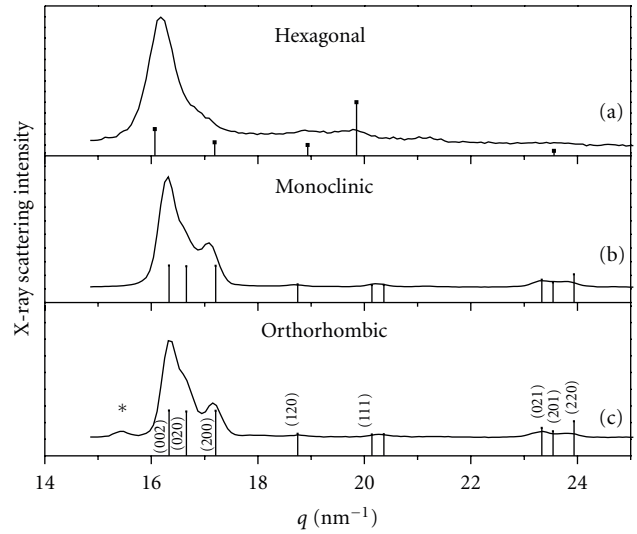

Figure 3: XRD patterns of tungsten oxide thin films prepared at 400, 500, 600°C indicating the formation of h-WO_3, m-WO_3, and o-WO_3. The peak at 15.5 nm^{-1}, indicated by *, is emerging from the ITO layer (c).

sample. From the TEM image, it can be observed that the film is composed of WO_3 nanocrystallites of an average size ~25 nm. The value of the interplanar distance is 0.3683 nm, which is the lattice parameter c of m-WO_3.

3.2. Crystalline Phases of the EC Layers Prepared at 400, 500, and 600°C. Raman spectra of the WO_3 film heat treated at 400 and 500°C are shown in Figures 2(a) and 2(b). For the films heat treated at 400°C, the bands below 200 cm^{-1} can be ascribed to lattice vibrations. The band observed at 251.4 cm^{-1} is assigned to δ(O-W-O) deformation vibrations, while the bands at 690.8 and 817.2 cm^{-1} are due to ν(O-W-O) stretching vibrations. These bands are characteristic features of h-WO_3. The Raman peak positions of our h-WO_3 films match those reported for h-WO_3 powder by Daniel et al. [21]. The bands at 817.2 and 690.8 cm^{-1} are broadened due to the nanocrystalline nature of the h-WO_3 films. Figure 2(b) shows the Raman spectrum of the films prepared at 500°C. The m-WO_3 features are observed from the Raman peaks at 134.0 cm^{-1} (lattice mode), 270.7 cm^{-1} δ(O-W-O), and ν(O-W-O) modes at 711.6 and 806.2 cm^{-1}.

The Raman spectrum (Figure 2(c)) of the WO_3-TiO_2 composite film heat treated at 600°C shows peaks at 806.2, 712.6 cm^{-1} (ν(O-W-O)), 328.1, 268.5 cm^{-1} (δ(O-W-O)), 133.6, 92.5 cm^{-1} (lattice modes) and a low intensity peak at 151.5 cm^{-1}. It is well known that the peak positions corresponding to the stretching vibrations of O-W-O bonds are the same for the triclinic, monoclinic, and orthorhombic phases of WO_3, whereas their lattice vibrations in the range 70–100 cm^{-1} show a difference in the Raman spectra [17, 22]. This is primarily due to the fact that the lattice vibrational bands arise from the $(W_2O_2)_n$ chains of WO_3. As the low temperature phases of WO_3 are less symmetric than the high-temperature phases, the lattice vibrations between 70 and 100 cm^{-1} in Figure 2(b) exhibit more Raman bands for the monoclinic phase (83.6, and 72.0 cm^{-1}) and only one mode at 92.5 cm^{-1} for the orthorhombic phase (Figure 2(c)).

Pecquenard et al. have shown that o-WO_3 can be crystallized at temperatures between 600 and 800°C using titanium oxide as structure stabilizer [22]. They reported the lattice vibrational mode of o-WO_3 at 91 cm^{-1}, which is similar to our result for the WO_3-TiO_2 composite film annealed at 600°C.

Figure 3(a) shows the X-ray scattering of the WO_3 layer, deposited on the ITO glass substrate and annealed at 400°C for one hour corresponds to hexagonal WO_3, for which the JCPDS card 85–2460 diffraction pattern is shown by the vertical bars [23]. By fitting the diffraction pattern, we find the lattice constants of the hexagonal phase to be a = 0.7379 ± 0.0008 and c = 0.7756 ± 0.0002 nm.

Figure 3(b) shows the diffraction pattern of the WO_3 film heat treated at 500°C. It matches with the JCPDS card 43–1035 diffraction pattern of pure m-WO_3 (vertical bars). The lattice parameters obtained from the fitting of the diffraction pattern are a = 0.7351 ± 0.0002, b = 0.75396 ± 0.0005, c = 0.7712 ± 0.0002 nm, with β = 90.3°. Although the peaks are similar in Figures 3(b) and 3(c), the lattice parameters obtained from the fitting for the sample annealed at 600°C are a = 0.7351 ± 0.0019, b = 0.7566 ± 0.0019, and c = 0.7724 ± 0.0021 nm, with β = 90° indicating that the WO_3 is in the orthorhombic phase.

3.3. Construction of Asymmetric Electrochromic Devices Based on h-WO_3, m-WO_3, and o-WO_3 Layers. In this section we describe the construction of asymmetric EC devices by using the thus synthesised h-WO_3, m-WO_3, and o-WO_3 thin films as the active electrochromic layer. The asymmetric EC device consists of an ion conductor layer, which also acts as a counter electrode and a WO_3 EC layer as the working cathode. These are sandwiched between two transparent conductive electrodes. As a low voltage is applied across the

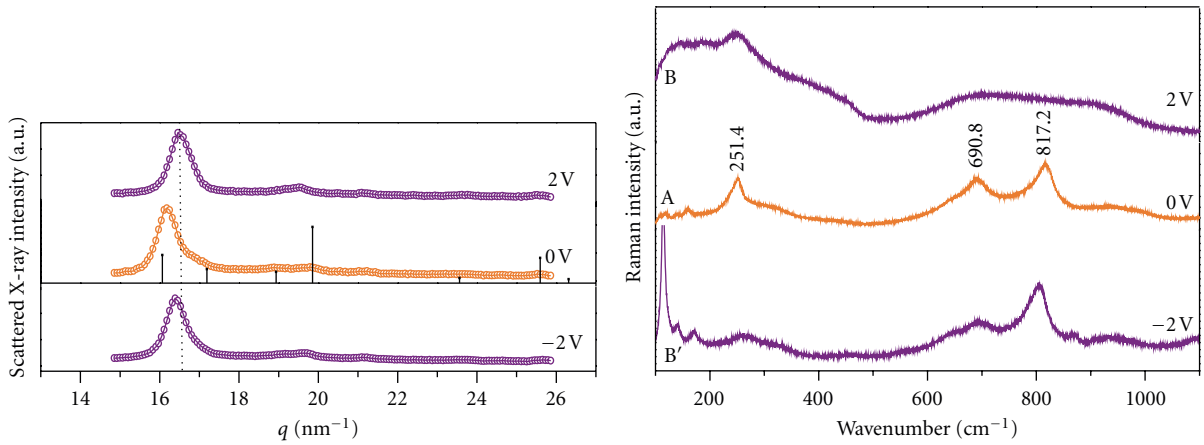

FIGURE 4: Electrochromic structural changes in the EC device constructed using h-WO_3 layer.

transparent conductors (1–3 V), ions move from the counter electrode and electrons from the transparent electrode to the EC layer to trigger a color change. The EC phenomenon occurring with such double injection can be represented as:

$$\underset{\text{clear}}{WO_3} + x\text{Li}^+ + xe^- \longleftrightarrow \underset{\text{dark blue}}{\text{Li}_x\text{WO}_3} \quad (3)$$

where x electrons (e^-) and lithium ions (Li^+) are inserted into or ejected from the system. Reversing the voltage restores the device to its previous clear (bleached) optical state. The ion conducting layer is a gel which is prepared by mixing lithium iodide (LiI) and iodine (I_2) in an ethanol solution with ORMOSIL. A network of silanes, present in ORMOSIL, acts as the ion storage layer. This ion conducting layer supplies Li^+ ions to the EC layer under proper biasing. This layer is applied on top of the WO_3 layer and another ITO-coated glass substrate is gently pressed against the ICL gel. The transparent conductive electrode (ITO layer) is 190 ± 40 nm thick. The thickness of the WO_3 layer used in the EC device was of 842 ± 50 nm. The 12 ± 1 μm thick ICL is sandwiched between the WO_3 layer and a second ITO coated-glass slide. Then the device is connected to the leads, and it is ready for the testing.

3.4. Electrochromic Structural Studies during Intercalation (Deintercalation) of Li^+ Ions into (Ejected out of) the h-WO_3 Layer of the EC Device. Figure 4 shows the XRD pattern (a) and the Raman spectrum (b) of the EC device constructed by using the h-WO_3 layer as an active working layer, in its colored and bleached states for applied potentials of 0.0 and ±2.0 V. Inserting and extracting lithium at ±2.0 V shift the diffraction peak positions as seen in the figure. The lattice parameters of the WO_3 EC layer at 0 V are a = 0.7379 ± 0.0008 and c = 0.7756 ± 0.0002 nm. We note that the lattice parameter c decreases to 0.76152 ± 0.0003 during the sequence of measurements. The observed variations in the lattice parameters of h-WO_3 EC layer upon lithiation are compared in the Table 1. The lattice parameter a remains initially the same, indicating that the unit cell volume decreases as the device ages during cycling. With an applied voltage of ±2.0 V, we observe that the lattice constant c is significantly lower for the Li-intercalated state (positive voltage) and that c increases as the lithium ions are extracted. The crystallite size remains generally close to 10 nm, with a possible slight increase during the measurement sequence.

Raman spectra show strong changes in the stretching bands. Figure 4(b)A shows the Raman spectrum of the pure h-WO_3 layer. The bands located at 251.4 cm^{-1}, due to δ(O-W-O), and at 690.8 and 817.2 cm^{-1} due to the ν(O-W-O), are the characteristic Raman modes of the h-WO_3. By applying a potential of 2.0 V across the device, Li ions are intercalated from ICL into the h-WO_3 layer. Figure 4(b)B shows the Raman spectrum of the EC device in its colored state after applying a voltage of 2.0 V. It can be seen that upon Li intercalation at this potential, the modes due to the ν(O-W-O) stretching vibrations disappear. Correspondingly, by reversing the potential (−2.0 V), the device reverts to its previous bleached state by deintercalating Li (Figure 4(b)B′), clearly demonstrating the structural reversibility of the active layer of the EC device.

A striking difference in the Raman spectra of h-Li_xWO_3 is the vanishing of bands at the applied coloration potentials of 2.0 V, although XRD pattern showed no structural transition. In order to understand the vanishing of the stretching ν(O-W-O) modes in the Raman spectra (Figure 4(b)B), while the EC active layer remains (h-Li_xWO_3) we consider the Li^+ occupancy for the applied potential of 2.0 V. In this scenario, Li ions inside the hexagonal windows (HW) start moving towards the four coordinated square window (SW) in order to accommodate the additional Li ions [9]. Hibino et al. have suggested that the location of Li ion near the SW is governed by the Li-Li ionic distances and the distance between the SW [24]. As there is no shielding for the Li ions and the Li-Li ionic distance is more than 5.5 Å, Li ions can only occupy alternate sites close to SW. This leads to ordering of Li ions inside the h-WO_3. Hibino et al. have mentioned that for Li/W ratios >0.4, the SWs of the h-WO_3

Table 1: The lattice parameters of WO_3 EC layer prepared at 400, 500, and 600°C and the lattice parameters after lithiating the sample at +2.0 V.

S. No.	Sample name	Coloration voltage	Lattice parameter nm			Angle
			a	b	c	β
1	400°C (Hexagonal)	0 V	0.7379 ± 0.0008	—	0.7756 ± 0.0002	—
		+2 V	0.74118 ± 0.0012		0.76152 ± 0.0003	
2	500°C (Monoclinic)	0 V	0.7351 ± 0.0002	0.7540 ± 0.0005	0.7712 ± 0.00019	90.3 ± 0.6
		+2 V	0.7397 ± 0.0015	0.7418 ± 0.002	0.7717 ± 0.0002	89.6 ± 10.1
3	600°C (Orthorhombic)	0 V	0.7351 ± 0.0019	0.7566 ± 0.0019	0.7724 ± 0.0021	90.0
		+2 V	0.7445 ± 0.0023	0.7469 ± 0.0058	0.7624 ± 0.0055	90.0

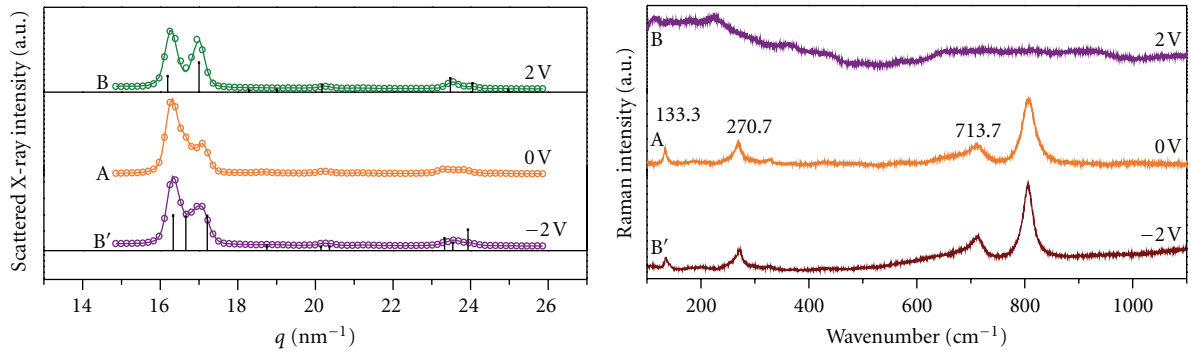

Figure 5: Electrochromic structural changes in the EC device constructed using m-WO_3 layer.

structure start to be occupied. In our case this happens when a coloration voltage of 2.0 V is applied to the EC device [24]. h-WO_3 is constituted by WO_6 octahedrons. The ab plane in WO_6 is already nearly symmetric. When Li is inserted into the square windows, the axial oxygen is also symmetrized, which results in isostructural WO_6 octahedra as in the cubic-ReO_3 structure. For this type of structure vibrations are not Raman active. Hence Raman modes vanish for the Li ion intercalation at a coloration potential of 2.0. A detailed account on the structural transformation of h-Li_xWO_3 is presented elsewhere [9].

3.5. Electrochromic Structural Studies during Intercalation (Deintercalation) of Li^+ Ions into (Ejected out of) the m-WO_3 Layer of the EC Device. Figure 5 shows the XRD pattern (a) and the Raman spectra (b) of the EC device constructed by using the m-WO_3 layer as an active working layer, in its colored and bleached states for applied potentials of 0.0 and ±2.0 V. The X-ray scattering of the Li_xWO_3 layer of the EC device based on the m-WO_3 layer is shown in Figure 5(a) as a function of the applied voltage. The diffraction pattern of the pure m-WO_3 layer, for which the JCPDS card 43–1035 diffraction pattern is represented by the vertical bars, is shown in Figure 5(a)B′. We determine the lattice constants *a, b,* and *c* and the angle β of the monoclinic phase for different sample states by fitting the diffraction patterns shown in Figure 5(a). The XRD pattern of the pure m-WO_3 layer has the lattice parameter $a = 0.7351 \pm 0.0002$, $b = 0.75396 \pm 0.0005$, $c = 0.7712 \pm 0.0002$ nm, with $\beta = 90.3°$. As the coloration voltages were applied, the XRD peaks change in the position and in the intensities indicating a structural transition associated with intercalation of Li. When a coloration potential of 2.0 V is applied, the *a* and *b* lattice parameters converge to a value of 0.7412 nm, while *c* parameter is 0.77165 nm. The XRD pattern of the Li_xWO_3 after Li intercalation resembles that of the tetragonal WO_3 crystalline phase (JCPDS 89–1287). The phase transition from m-WO_3 to tetragonal Li_xWO_3 (t-Li_xWO_3) is obtained. It should be noted that, when the Li ions are deintercalated by applying reverse potential, the crystalline structure of m-WO_3 layer reverts back to the initial monoclinic lattice as shown in Figure 5(a)(B′). The observed variations in the lattice parameters of m-WO_3 EC layer upon lithiation are compared in the Table 1.

Figure 5(b) A shows the Raman spectrum of the pure m-WO_3 layer. The Raman peaks at 713.7 and 806.2 cm^{-1}, attributed to ν(O-W-O) modes of m-WO_3, were followed during the EC coloration and bleaching at ±2.0 V. Figure 5(b)B shows the Raman spectrum of the m-WO_3 layer, coloured at 2.0 V. The Raman modes due to ν(O-W-O) vanish completely. It has been observed from our previous work on XRD of Li_xWO_3 layer that for the applied coloration potential of 1.0 V, the lattice parameter *c* decreases from 0.77418 ± 0.0002 nm to 0.7717 ± 0.00015 nm. At the same time, the lattice parameters *a* (= 0.7397 ± 0.00145 nm) and *b* (= 0.7418 ± 0.0021 nm) converge to a same value within the

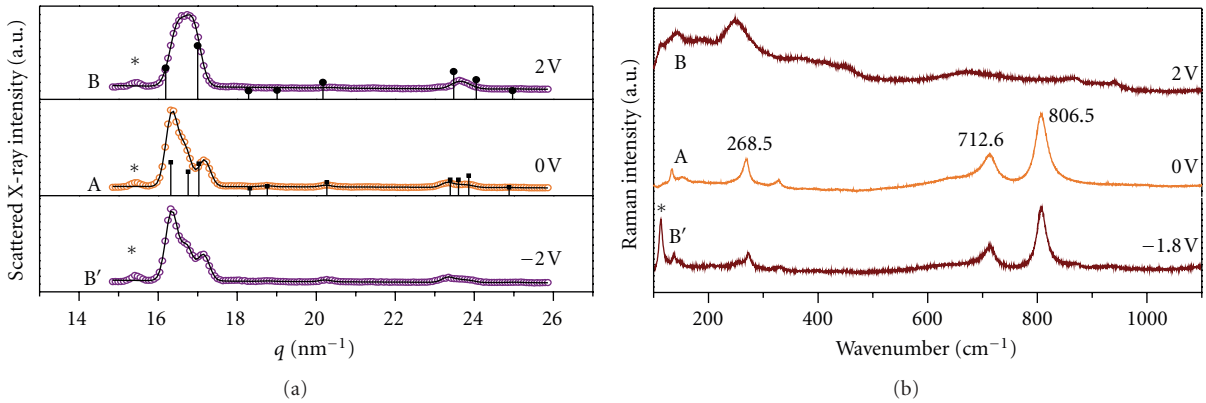

Figure 6: Electrochromic structural changes in the EC device constructed using o-WO_3 layer.

experimental error. This tendency of c to converge towards a and b indicates that the system is moving towards a cubic phase as the amount of intercalated Li is increased. The vanishing of the Raman mode is also attributed to this trend of Li_xWO_3 system to move towards cubic phase. It has been reported that the cubic Li_xWO_3 phase was obtained for $x > 0.5$ [5, 16]. In our case, Li intercalation into WO_3 at 2.0 V is not sufficient to reach cubic phase, whereas a higher symmetric state than that of the tetragonal phase is clearly observed. This indicates that for the applied potential of 2.0 V the amount of Li that has intercalated into m-WO_3 is between 0.23 and 0.5. The complete vanishing of ν(O-W-O) Raman modes observed at a coloration potential of +2.0 V is attributed to a phase transition to a higher symmetric state than that of t-Li_xWO_3. Also, it is possible that atomic displacement within the unit cell could take place with the same lattice parameters, as Raman spectroscopy is sensitive even to a small change in the lattice parameters. Figure 5(b)B′ shows the Raman spectrum of the m-WO_3 layer of the EC device after the deintercalation of Li at −2.0 V. The recorded Raman spectra exhibit the spectral features of the initial pure m-WO_3 layer (Figure 5(b)A). This demonstrates the structural EC reversibility of the system.

3.6. Electrochromic Structural Studies during Intercalation (Deintercalation) of Li^+ Ions into (out of) the o-WO_3 Layer of an EC Device. Figure 6(a) shows the X-ray scattering of the Li^+ intercalated/deintercalated o-WO_3 layer in a working EC device for applied potentials of ±2.0 V. The differences in the positions and intensity of the diffraction lines observed in Figure 6(a) show the structural changes associated with Li ion intercalation/deintercalation. The XRD pattern of Li ion deintercalated state is similar to that of the o-WO_3 state at 0 V. The lattice parameters of the o-WO_3 layer calculated from the fitting of the XRD patterns are $a = 0.7351 \pm 0.0019$, $b = 0.7566 \pm 0.0019$, and $c = 0.7724 \pm 0.0021$ nm, with $\beta = 90°$. Upon applying a coloration potential of 2.0 V, a transition to the t-Li_xWO_3 phase is obtained. At this potential, the lattice parameters a and b attain about the same value ($a = 0.7445 \pm 0.0023$, $b = 0.7469 \pm 0.0058$ nm), whereas c is reduced to 0.7624 ± 0.0055 nm. The observed variations in the lattice parameters of titania stabilized o-WO_3 EC layer, upon lithiation, are compared in the Table 1. This observed structural change is consistent with the well-established Li-induced phase transitions of low- to high-symmetric phases in ReO_3-type tungsten oxides [16, 17, 19]. Upon lithium intercalation, the low-symmetry phases of WO_3, such as triclinic and monoclinic, transform to higher symmetry structures such as tetragonal and cubic [16, 17, 19]. In this work, upon lithium ion intercalation, we have observed the phase transition from o-WO_3 to t-Li_xWO_3, the next higher symmetric phase. In this tetragonal phase the "ab" plane of the WO_6 octahedron is symmetric, a transformation induced by Li ion intercalation at 2.0 V. At this potential, the Li ion concentration is 0.226 and a complete phase transformation to the t-Li_xWO_3 is achieved. These values of Li ion concentrations for the observed phases are consistent with the values reported by other authors [16, 19]. The phase transition as a function of the applied potential occurs gradually from o-WO_3 to t-Li_xWO_3 with a tendency for a phase transition towards a cubic Li_xWO_3, as the concentration of the inserted Li ions increases from 0.090 to 0.226.

Figure 6(b) shows the Raman spectra of the o-WO_3 layer in a working EC device as a function of applied voltage. When a coloration potential of 2.0 V is applied, all the O-W-O stretching modes vanish (Figure 6(b)B), as expected for the more symmetric phases. The XRD analysis shows that the phase transition occurs gradually, and it is impossible to clearly identify the phase of the Li_xWO_3; since the lattice parameters are changing continuously as a function of applied potential or in other words, as a function of the amount of intercalated Li ions. The Raman spectrum in Figure 6(b)B shows no O-W-O stretching modes due to the fact that the structure of the o-WO_3 layer is gradually becoming more symmetric. In a previous work, we have shown that for higher voltages such as 3.0 V, the Li_xWO_3 attains a cubic phase when starting from the m-WO_3 phase and that all the Raman modes vanished [5]. Figure 6(b)B′ show that the o-WO_3 crystalline structure is recovered, when the coloring voltage is reversed (−2.0 V), demonstrating the reversibility of the device. The detailed report on the performance of the o-WO_3 layer as EC active layer is presented in our previous paper [25].

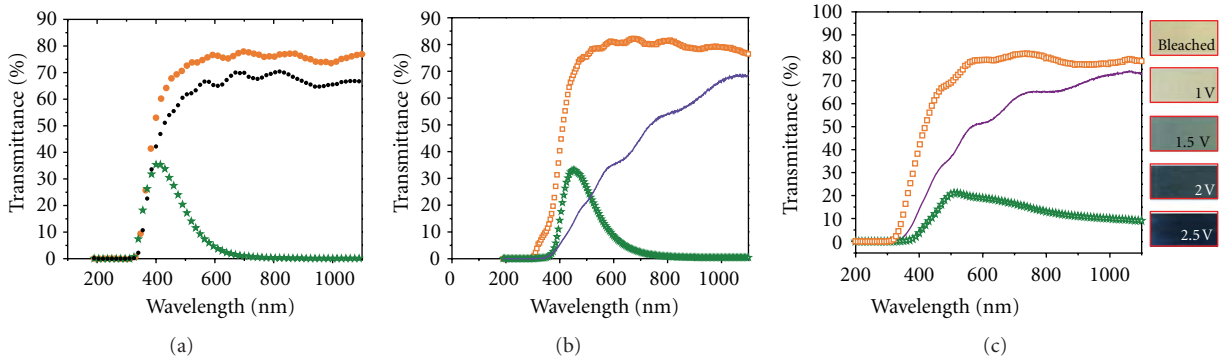

FIGURE 7: Transmission spectra of the EC devices constructed using h-WO_3, m-WO_3, and o-WO_3 in the as prepared state, at coloration potential of 2.5 V and at bleaching potential of −1.0 V. The photos show the visible coloration to the naked eye when the EC devices are colored at various coloration potential. The photos represent typically the EC device based on m-WO_3.

3.7. Optical Studies of the Electrochromic Devices Based on the h-WO_3, m-WO_3, and o-WO_3 Layers. The optical transmittance of the EC device constructed by using the h-WO_3, layer in its colored and bleached states for an applied coloration potential of 2.5 V and at bleaching potential of −1.0 V is shown in Figure 7(a). The recorded transmission spectra of the device in the bleached state for potentials at −2.5 V are indistinguishable from the spectrum of the device bleached at −1.0 V (hence not shown), clearly demonstrating the reversibility of the device. In the bleached state, the transmittance of the device at a wavelength 1100 nm was 76.9%. At +2.5 V the transmittance is reduced 0.1%. When the coloration potentials of +2.5 V are applied, the maximum transmittance is observed at 403.5 nm, and the transmittance FWHM is 147.0 nm. The optical modulation of ~76% above 800 nm obtained here is exceptionally high for EC devices [26]. Figure 7(b) shows the optical transmittance spectra of a m-WO_3-(prepared at 500°C) based EC device in bleached state (−1.0 V) and coloured at +2.5 V. In the bleached state, the transmittance of the device at 1100 nm was 76.4%. At the coloration potential of +2.5 V the transmittance was reduced to 0.0%. The device exhibits an optical modulation of 76.1%. Figure 7(c) shows the transmission spectra of the o-WO_3, based EC device in its colored and bleached states. In the bleached state the transmittance at a wavelength of 1100 nm was 78.5%. At a coloration potential of +2.5 V the corresponding transmittance is reduced to 9.1%. The actual digital photograph images of the device in the bleached and colored states for the device prepared using m-WO_3 (i.e, EC layer prepared at 500°C) are also presented in Figure 7. The optical modulation of about ~70% or more obtained in the EC devices constructed in this work is highly desirable for practical applications in electrochromic smart windows. Further, the transmittance of the mesomacroporous WO_3 layer (solid line) is lower than the bleached transmission spectrum of the device, which is attributed to the volume scattering in the film due to the microstructure [27].

4. Summary

Various mesomacroporous, crack-free, nanocristalline (NC) WO_3 thin films up to ~850 nm thick were prepared using tungstic acid as a precursor and ORMOSIL as a templating agent. Pure h-WO_3 NC films with crystallite size of ~10 nm were obtained after calcination at 400°C. Pure m-WO_3 films with crystallite size of ~16 nm were synthesized after annealing at 500°C. o-WO_3 thin films, stabilized by NC anatase TiO_2, are obtained by a sol-gel-based two-stage dip coating method and subsequent annealing at 600°C. Thus prepared WO_3 films on ITO coated glass substrate were used as the active EC layer for the construction of various asymmetric EC devices. Coloration and bleaching of the EC devices were achieved by intercalating and deintercalating Li into the WO_3 layers at coloration potential of 2.5 V and at bleaching potential of −1.0 V. The EC devices based on h-WO_3, m-WO_3, and o-WO_3 as EC active layers exhibit an exceptionally high optical modulation of 70% and qualify the device for EC smart window applications.

Acknowledgment

The financial support of the National Science and Engineering Research Council (NSERC) of Canada is gratefully acknowledged.

References

[1] E. Rossinyol, A. Prim, E. Pellicer et al., "Synthesis and characterization of chromium-doped mesoporous tungsten oxide for gas-sensing applications," *Advanced Functional Materials*, vol. 17, no. 11, pp. 1801–1806, 2007.

[2] T. He and J. Yao, "Photochromic materials based on tungsten oxide," *Journal of Materials Chemistry*, vol. 17, no. 43, pp. 4547–4557, 2007.

[3] C. G. Granqvist, "Out of a niche," *Nature Materials*, vol. 5, no. 2, pp. 89–90, 2006.

[4] S. K. Deb, "Opportunities and challenges in science and technology of WO_3 for electrochromic and related applications," *Solar Energy Materials and Solar Cells*, vol. 92, no. 2, pp. 245–258, 2008.

[5] C. G. Granqvist, "Electrochromic tungsten oxide films: review of progress 1993–1998," *Solar Energy Materials and Solar Cells*, vol. 60, no. 3, pp. 201–262, 2000.

[6] E. Stathatos, P. Lianos, U. Lavrencic-Stangar, and B. Orel, "A high-performance solid-state dye-sensitized photoelectrochemical cell employing a nanocomposite gel electrolyte made by the sol-gel route," *Advanced Materials*, vol. 14, no. 5, pp. 354–357, 2002.

[7] P. R. Somani and S. Radhakrishnan, "Electrochromic materials and devices: present and future," *Materials Chemistry and Physics*, vol. 77, no. 1, pp. 117–133, 2003.

[8] S. Balaji, A.-S. Albert, Y. Djaoued, and R. Brüning, "Micro-Raman spectroscopic characterization of a tunable electrochromic device for application in smart windows," *Journal of Raman Spectroscopy*, vol. 40, no. 1, pp. 92–100, 2009.

[9] S. Balaji, Y. Djaoued, A.-S. Albert, R. Z. Ferguson, and R. Brüning, "Hexagonal tungsten oxide based electrochromic devices: spectroscopic evidence for the Li ion occupancy of four-coordinated square windows," *Chemistry of Materials*, vol. 21, no. 7, pp. 1381–1389, 2009.

[10] S.-H. Baeck, K. S. Choi, T. F. Jaramillo, G. D. Stucky, and E. W. McFarland, "Enhancement of photocatalytic and electrochromic properties of electrochemically fabricated mesoporous WO_3 thin films," *Advanced Materials*, vol. 15, no. 15, pp. 1269–1273, 2003.

[11] W. Cheng, E. Baudrin, B. Dunn, and J. I. Zink, "Synthesis and electrochromic properties of mesoporous tungsten oxide," *Journal of Materials Chemistry*, vol. 11, no. 1, pp. 92–97, 2001.

[12] Y. Djaoued, P. V. Ashrit, S. Badilescu, and R. Brüning, "Synthesis and characterization of macroporous tungsten oxide films for electrochromic application," *Journal of Sol-Gel Science and Technology*, vol. 28, no. 2, pp. 235–244, 2003.

[13] C. Santato, M. Odziemkowski, M. Ulmann, and J. Augustynski, "Crystallographically oriented mesoporous WO_3 films: synthesis, characterization, and applications," *Journal of the American Chemical Society*, vol. 123, no. 43, pp. 10639–10649, 2001.

[14] Y. Djaoued, S. Priya, and S. Balaji, "Low temperature synthesis of nanocrystalline WO_3 films by sol-gel process," *Journal of Non-Crystalline Solids*, vol. 354, no. 2–9, pp. 673–679, 2008.

[15] C. G. Granqvist, *Handbook of Inorganic Electrochromic Materials*, Elsevier, New York, NY, USA, 1995.

[16] Q. Zhong, J. R. Dahn, and K. Colbow, "Lithium intercalation into WO_3 and the phase diagram of Li_xWO_3 ," *Physical Review B*, vol. 46, no. 4, pp. 2554–2560, 1992.

[17] A. Kuzmin, J. Purans, E. Cazzanelli, C. Vinegoni, and G. Mariotto, "X-ray diffraction, extended x-ray absorption fine structure and Raman spectroscopy studies of WO_3 powders and (1-x)WO3-y·xReO2 mixtures," *Journal of Applied Physics*, vol. 84, no. 10, pp. 5515–5524, 1998.

[18] O. Pyper, A. Kaschner, and C. Thomsen, "In situ Raman spectroscopy of the electrochemical reduction of WO_3 thin films in various electrolytes," *Solar Energy Materials and Solar Cells*, vol. 71, no. 4, pp. 511–522, 2002.

[19] E. Cazzanelli, C. Vinegoni, G. Mariotto, A. Kuzmin, and J. Purans, "Low-temperature polymorphism in tungsten trioxide powders and its dependence on mechanical treatments," *Journal of Solid State Chemistry*, vol. 143, no. 1, pp. 24–32, 1999.

[20] T. Kudo, "A new heteropolyacid with carbon as a heteroatom in a Keggin-like structure," *Nature*, vol. 312, no. 5994, pp. 537–538, 1984.

[21] M. F. Daniel, B. Desbat, J. C. Lassegues, B. Gerand, and M. Figlarz, "Infrared and Raman study of WO_3 tungsten trioxides and WO_3, xH_2O tungsten trioxide tydrates," *Journal of Solid State Chemistry*, vol. 67, no. 2, pp. 235–247, 1987.

[22] B. Pecquenard, H. Lecacheux, J. Livage, and C. Julien, "Orthorhombic WO_3 formed via a Ti-stabilized $WO_3 \cdot 1/3H_2O$ phase," *Journal of Solid State Chemistry*, vol. 135, no. 1, pp. 159–168, 1998.

[23] *Powder Diffraction Files Inorganic and Organic (Card No: 85-2460 (Hexagonal-WO3)*, JCPDS-International Centre for Diffraction Data, PDF2 Data Base, Swarthmore, Pa, USA, 1996.

[24] M. Hibino, W. Han, and T. Kudo, "Electrochemical lithium intercalation into a hexagonal WO_3 framework and its structural change," *Solid State Ionics*, vol. 135, no. 1–4, pp. 61–69, 2000.

[25] S. Balaji, Y. Djaoued, A. S. Albert, R. Brüning, N. Beaudoin, and J. Robichaud, "Porous orthorhombic tungsten oxide thin films: synthesis, characterization, and application in electrochromic and photochromic devices," *Journal of Materials Chemistry*, vol. 21, no. 11, pp. 3940–3948, 2011.

[26] C. G. Granqvist, E. Avendaño, and A. Azens, "Electrochromic coatings and devices: survey of some recent advances," *Thin Solid Films*, vol. 442, no. 1-2, pp. 201–211, 2003.

[27] C. Amra, "From light scattering to the microstructure of thin-film multilayers," *Applied Optics*, vol. 32, no. 28, pp. 5481–5491, 1993.